Electronic Supplementary Information

Luminescent Single-Molecule Magnet of Dimetallofullerene with Cage-Dependent Property

Mingzhe Nie,[a, d] Le Yang,[c] Chong Zhao,[a, d] Haibing Meng,[a, d] Lai Feng,[b] Peng Jin,*[c]*

Chunru Wang,[a] Taishan Wang*[a]*

[a]Beijing National Laboratory for Molecular Sciences, Key Laboratory of Molecular Nanostructure and Nanotechnology, Institute of Chemistry, Chinese Academy of Sciences, Beijing 100190, China

[b]Soochow Institute for Energy and Materials InnovationS, College of Physics, Optoelectronics and Energy & Jiangsu Key Laboratory of Advanced Carbon Materials and Wearable Energy Technologies, Soochow University, Suzhou 215006, China

[c]School of Materials Science and Engineering, Hebei University of Technology, Tianjin 300130, China

[d]University of Chinese Academy of Sciences, Beijing 100049, China

E-mail: wangtais@iccas.ac.cn (T. W.); fenglai@suda.edu.cn (L. F.); china.peng.jin@gmail.com (P. J.); crwang@iccas.ac.cn (C. W.).

Experimental methods

Synthesis and characterization. DyEr@C_{82} metallofullerenes were synthesized by arc-discharging method, the mixture of graphite powder and metal alloy (molar ratio of Er/Ni: Dy/Ni alloy = 1: 1) were packed into core-drilled graphite rods. Subsequently, the rods of three types were vaporized in a Krätschmer-Huffman generator under an atmosphere of 200 Torr He. The as-prepared soot was Soxlet-extracted with toluene for 24 h, and then the concentrated toluene solution was filtered for HPLC purification, the isolation was performed by multistep HPLC. The purity was determined by high resolution matrix-assisted laser desorption ionization time-of-flight (MALDI-TOF) mass spectrum (Autoflex, Bruker).

Magnetic measurements. Magnetic properties were determined using *Quantum Design MPMS3 VSM* magnetometer. The sample was prepared by drop-casting from carbon disulfide solution onto a slice of Al foil, fast evaporation of carbon disulfide afforded black powder. Then the Al foil was folded into a small cube with sample packaged in it. Finally, the cube was stuck on the wall of a straw with very small amount of M grease. The mass of DyEr@C_s-C_{82} and DyEr@C_{3v}-C_{82} were 0.56 mg and 0.5 mg, respectively. Al foil and molecular formula (Pascal constant) were considered when correction was carried out on the data. The M grease was not considered since the mass of it was hard to be determined. The data of hysteresis and ZFC/FC were collected using VSM mode, while the other data were collected using dc mode. In magnetization decay experiments, a field of 10000 Oe was applied to magnetizing the samples and was removed as fast as possible (700 Oe/s). The remanent field is a negative one. The relaxation times were obtained by fitting the data using equation S1, where M_{eq}, τ and b are fitting parameters.

$$M(t) = M_{eq} + (M_0 - M_{eq})exp[-\left(t/\tau\right)^b] \quad \text{(S1)}.$$

Time-dependent dc magnetization decay measurements were performed on the powder sample of DyEr@C_{3v}-C_{82} to determine the relaxation time. The relaxation time showed an obvious linear relationship from 2 K to 7 K, Arrhenius fitting of linear regime affords an effect barrier U_{eff} of 6.4 K, pre-exponential factor τ_0 of 2.7 s.

Single-crystal X-ray Diffraction. Black block crystals of DyEr@C_{3v}-C_{82}·Ni^{II}(OEP) were obtained by slow diffusion of a toluene solution of Ni^{II}(OEP) (1 mg/mL, 2 mL) into a carbon disulfide solution of (1 mg/mL, 1 mL). X-ray diffraction data were collected at 153 K using a diffractometer (Rigaku Saturn724+) equipped with a CCD collector. Multi-scan method was used for absorption correction. The structure was resolved using direct methods (SIR2004) and refined on F^2 anisotropically by full-matrix least-squares using SHELXL2014 within the WinGX package. Hydrogen atoms were inserted at calculated positions and constrained with isotropic thermal parameters. Hydrogen atoms were inserted at calculated positions and constrained with isotropic thermal parameters. CCDC 1935179 contains the supplementary crystallographic data.

Crystallographic data and structure refinement parameters for DyEr@C_{3v}-C_{82}·Ni^{II}(OEP): Mr =1998.17, 0.2×0.1×0.2 mm^3, monoclinic, *C* 2/m (No.12), a = 25.2129(4), b = 14.9535(3), c = 20.2524(5), β = 97.136(2) °, V = 7576.4 $Å^3$, Z = 4, ρ_{calcd} = 1.752 g cm^{-3}, $\mu(MoK_\alpha)$ = 2.387 mm^{-1}, ϑ = 1.858~30.667, T = 110(2) K, R_1 =0.1053, wR_2 = 0.2717 for all data; R_1 = 0.0917, wR_1 = 0.2588 for 9004 reflections (I> 2.0σ(I)) with 1097 parameters. Goodness of fit indicator 1.002. Maximum residual electron density 2.409 e $Å^{-3}$.

Computational Methods. Full geometry optimizations were carried out by using the M06-2X[1] functional and the standard 6-31G* all-electron basis set for C[2, 3] and the Stuttgart/Dresden relativistic effective core potential[4] and corresponding basis set for the metals (denoted as M06-2X/6-31G*~SDD). All the DFT calculations were performed using the Gaussian 09 software. [5] Wiberg bond order (WBO), Mayer bond order (MBO) and Fuzzy bond order (FBO) were calculated by using the Multiwfn program.[6] The results were visualized using the CYLview[7] and VMD[8] softwares.

Detailed analysis of the metal-metal bond composition in the two DyEr@C_{82} isomers was carried out. As clearly shown in the Figure S9, the singly bonding MOs (DyEr@C_s(6)-C_{82}: α-HOMO-4, DyEr@C_{3v}(8)-C_{82} : α-HOMO) are hybrid orbitals from the metal- 6*s*, 6*p* and 5*d* atomic orbitals. The shared electron on this MO may stem from the Er-4*f* electrons, as indicated by the greatly reduced population on the Er 4*f* orbitals ($4f^{12}$->$4f^{11}$, Table 3).

In addition, the lowest unoccupied molecular orbitals (LUMOs) of DyEr@C_{82} are also visualized in Figure S9. The LUMOs of DyEr@C_s(6)-C_{82} are mainly localized on the carbon cage. For comparison, the α-LUMO of DyEr@C_{3v}(8)-C_{82} is localized on the carbon cage, whereas β-LUMO is mainly between the two metal atoms.

The explicit consideration of 4f electrons as valence electrons is common in the theoretical studies on the Dy and Er-based EMFs.[9-11] All the calculations were also repeated using ECP with all the metal-4*f* electrons as core (ECP56MWB for Dy/ECP58MWB for Er, http://www.tc.uni-koeln.de/PP/clickpse.en.html). Table S3 shows that both DyEr@C_s(6)-C_{82} and DyEr@C_{3v}(8)-C_{82} have the triplet ground-state structures at this level of theory. Figure S10 shows that DyEr@C_s(6)-C_{82} (α-HOMO-1) and DyEr@C_{3v}(8)-C_{82} (α-HOMO-1) both have a singly occupied bonding orbital between Dy and Er, suggesting the possible presence of a 1e-2c Dy-Er bond. Each metal atom donates two 6s electrons, and three of the four electrons transfer to the cage with another one kept between the Dy and Er atoms, forming the metal-metal bond. Consistent with this analysis, the spin densities of DyEr@C_{82} are mainly distributed on the cage (C_{82}^{3-}) and the region between Dy and Er.

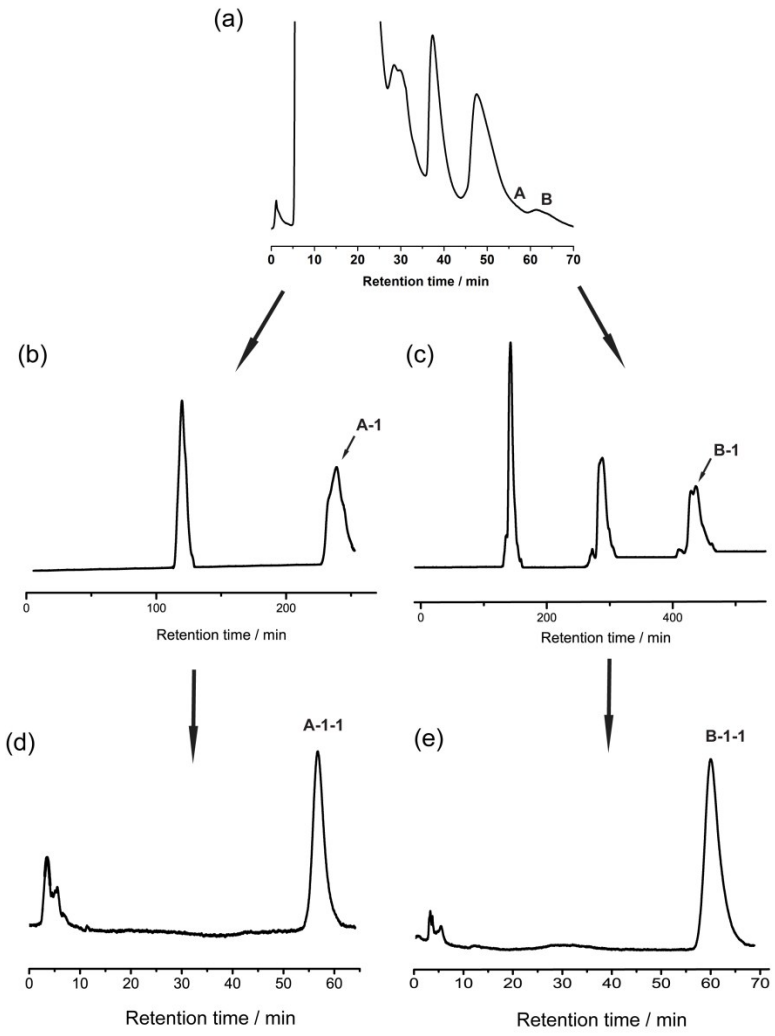

Figure S1. (a) HPLC profile of extract mixtures from fullerene raw soot in a 10×250 mm Buckyprep column, 12 mL/min flow rate with toluene as eluent phase. Fraction A and B was collected. (b) (c) Recycling HPLC profile of fraction A and B in a 10×250 mm Buckyprep column, 6 mL/min flow rate with toluene as eluent phase. Fraction A-1 and B-1 was collected. (d)(e) HPLC profile of fraction A-1-1 and B-1-1 in a 10×250 mm Buckyprep column, 12 mL/min flow rate with toluene as eluent phase. Fraction A-1-1 (DyEr@C_s-C_{82}) and B-1-1(DyEr@C_{3v}-C_{82}) were collected.

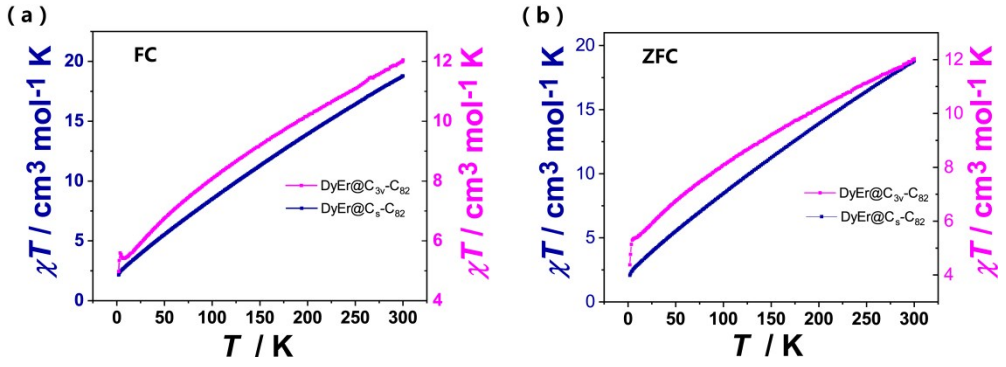

Figure S2. Plots of temperature dependence of $\chi_m T$ for powder samples of DyEr@C_{82} isomers.

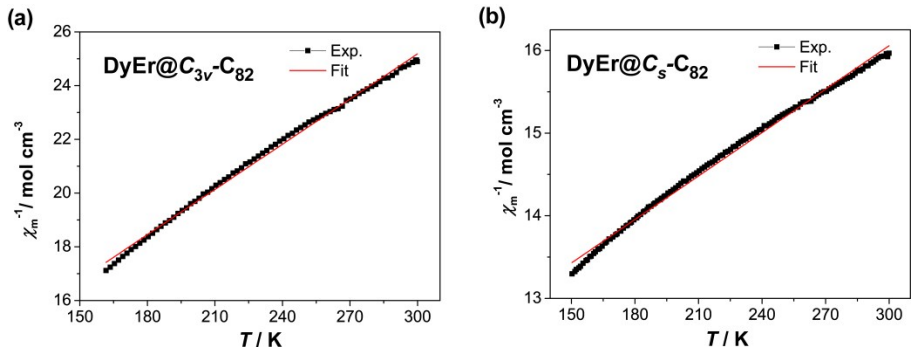

Figure S3. Experimental and simulated plots of χ_m^{-1} for powder samples of DyEr@C_{82} isomers.

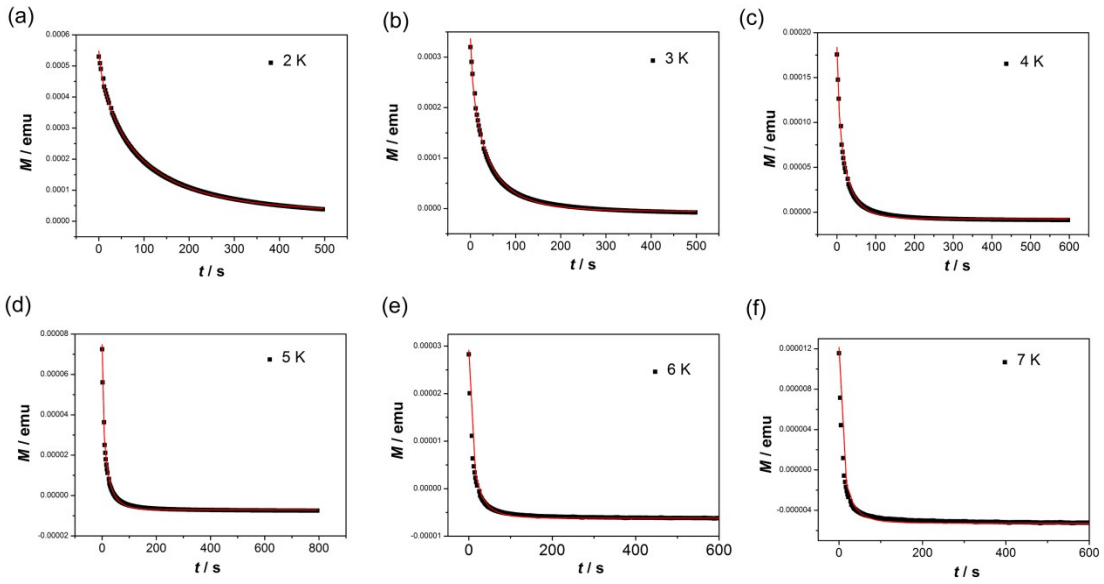

Figure S4. (a-f) Plots of time dependent magnetization decay for DyEr@C_{3v}-C_{82} under 2 to 7 K under zero field.

Table S1. The relaxation times obtained by fitting the plot of time dependent magnetization decay of DyEr@C_{3v}-C_{82}, where M_{eq}, τ and b are fitting parameters.

***T* / K**	M_{eq}	M_0	**τ / s**	***b***
2	2.63E-5	5.48E-4	83.5	0.71
3	-5.39E-6	3.36E-4	30.7	0.69
4	-7.68E-6	1.84E-4	16.6	0.69
5	-7.09E-6	7.47E-5	11.3	0.63
6	-6.2E-6	2.92E-5	9.7	0.62
7	-5.3E-6	1.21E-5	9.2	0.62

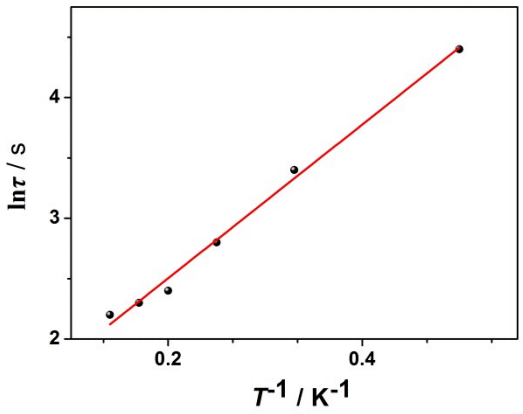

Figure S5. Plot of the logarithm of the relaxation time (ln(τ)) vs. reciprocal temperature (T^{-1}) of DyEr@C_{3v}-C_{82}. Red solid line shows the Orbach fitting of linear region. Fitting equation is $\ln \tau = \ln \tau_0 + U_{eff} / kT$.

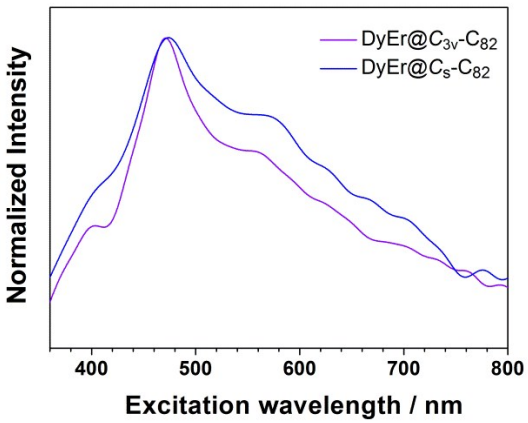

Figure S6. Photoluminescence excitation spectra of DyEr@C_s-C_{82} and DyEr@C_{3v}-C_{82} in CS_2 solution at 77 K (emission wavelength: 1520 nm).

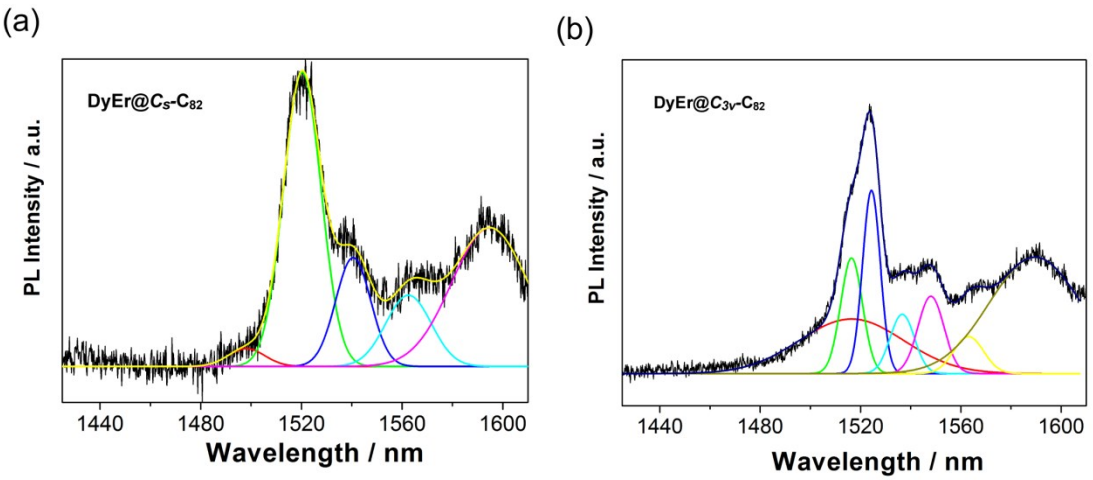

Figure S7. Fitting curves of photoluminescence spectra of (a) DyEr@C_s-C_{82} and (b) DyEr@C_{3v}-C_{82}.

Table S2. Relative energies (kcal/mol) of DyEr@C_{82} with different spin multiplicities (*M*).

M	5	7	9	11
DyEr@C_s(6)-C_{82}	14.8	9.1	**0.0**	16.2
DyEr@C_{3v}(8)-C_{82}	61.6	26.5	2.2	**0.0**

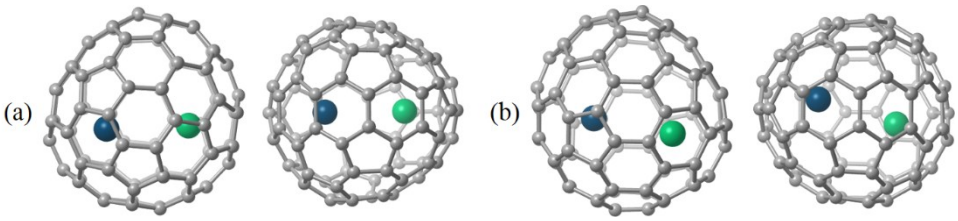

Figure S8. Optimized ground-state structures of (a) DyEr@C_s(6)-C_{82} and (b) DyEr@C_{3v}(8)-C_{82} (two views; Dy: blue; Er: green).

Table S3. Relative energies (kcal/mol) of DyEr@C_{82} with different spin multiplicities (*M*) at M06-2X/6-31G*~SDD (ECP56MWB for Dy/ECP58MWB for Er) level of theory.

M	1	3	5	7	9	11
DyEr@C_s(6)-C_{82}	16.4	**0.0**	27.5	78.9	146.9	202.3
DyEr@C_{3v}(8)-C_{82}	11.1	**0.0**	31.5	70.3	136.9	204.4

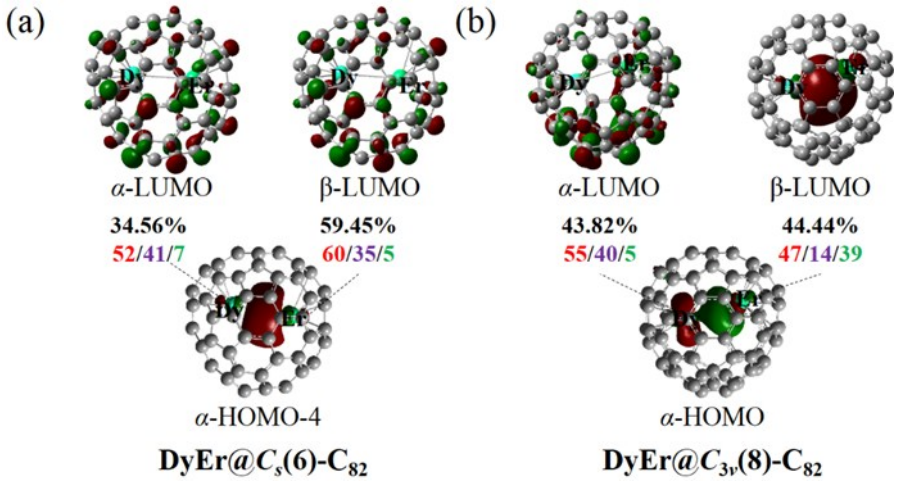

Figure S9. LUMOs and metal-metal bonding orbitals of (a) DyEr@C_s(6)-C_{82} and (b) DyEr@C_{3v}(8)-C_{82}. The participation (%) of Dy and Er AOs is first given in the same row, followed by the contribution (%) of the 6*s* (red), 6*p* (purple) or 5*d* (green) AOs to this metal hybrid orbital.

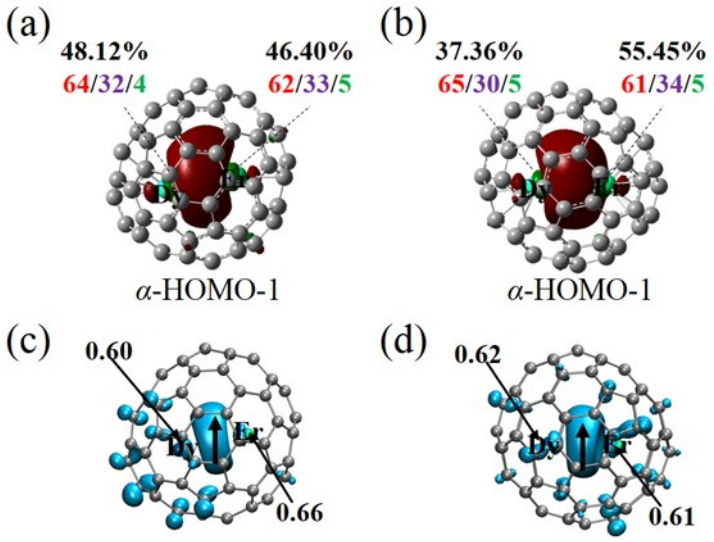

Figure S10. Metal-metal bonding orbitals of (a) DyEr@C_s(6)-C_{82} and (b) DyEr@C_{3v}(8)-C_{82}. The participation (%) of Dy and Er AOs is first given in the same row, followed by the contribution (%) of the 6*s* (red), 6*p* (purple) or 5*d* (green) AOs to this metal hybrid orbital. Spin density distributions (with spin population value for each metal atom) of (c) DyEr@C_s(6)-C_{82} and (d) DyEr@C_{3v}(8)-C_{82}. The spin of the single electron shared between the two metals are also shown.

References

1. Y. Zhao and D. G. Truhlar, *Theor. Chem. Acc.*, 2008, **120**, 215-241.

2. G. A. Petersson and M. A. Al‐Laham, *J. Chem. Phys.*, 1991, **94**, 6081-6090.

3. G. A. Petersson, A. Bennett, T. G. Tensfeldt, M. A. Al‐Laham, W. A. Shirley and J. Mantzaris, *J. Chem. Phys.*, 1988, **89**, 2193-2218.

4. X. Cao and M. Dolg, *Journal of Molecular Structure: THEOCHEM*, 2002, **581**, 139-147.

5. M. Frisch, G. Trucks, H. Schlegel, G. Scuseria, M. Robb, J. Cheeseman, G. Scalmani, V. Barone, B. Mennucci and G. Petersson, *Gaussian 09, Revision A.01, Gaussian, Inc., Wallingford CT, 2009*.

6. T. Lu and F. Chen, *J. Comput. Chem.*, 2012, **33**, 580-592.

7. C. Legault, , CYLview, 1.0b, Université de Sherbrooke, 2009.

8. W. Humphrey, A. Dalke and K. Schulten, *J. Mol. Graphics*, 1996, **14**, 33-38.

9. J. Wang, Y.-y. Zhao, P.-H. Lee and S. Irle, *Inorg. Chem.*, 2017, **56**, 6576-6583.

10. A. Velloth, Y. Imamura and M. Hada, *Inorg. Chem.*, 2019, **58**, 1208-1215.

11. S. Hu, W. Shen, L. Yang, G. Duan, P. Jin, Y. Xie, T. Akasaka and X. Lu, *Chem. – A Eur. J.*, 2019, **25**, 11538-11544.